Journal of Applied Geophysics xxx (2010) xxx–xxx

Contents lists available at ScienceDirect

Journal of Applied Geophysics

journal homepage: www.elsevier.com/locate/jappgeo

An application of the synthetic emitter-array method to improve GPR signals

Lorena Cedrina, Néstor Bonomo *, Ana Osella

Departamento de Física, Facultad de Ciencias Exactas y Naturales, Universidad de Buenos Aires, Ciudad Universitaria, Pabellón 1, (1428) Buenos Aires, Argentina
CONICET, Consejo Nacional de Investigaciones Científicas y Técnicas, Argentina

ARTICLE INFO

Article history:
Received 1 December 2008
Accepted 19 January 2010
Available online xxxx

Keywords:
GPR
Emitter-array method
Archaeology

ABSTRACT

Methods that employ arrays of emitters are potentially useful in improving weak or ambiguous signals in ground penetrating radar (GPR) prospecting. As in the seismic case, the electromagnetic responses from the subsurface can be obtained by employing true composite sources or synthesized from single emitter responses that are acquired with variable offset, both possibilities leading to similar results. In this article, the synthetic emitter-array method is examined as a way of improving GPR signals. Modeling of transmitted wave-fronts is carried out to analyze how the targets can be illuminated so that the reflected signals are effectively reinforced. The method is applied to different targets. A methodology that simultaneously increases the signal to noise ratio and the lateral coherence of the events is examined in order to facilitate the interpretation of the GPR data. Finally, the synthetic emitter-array method is successfully applied in a case study to determine the width and depth of mud walls at the Palo Blanco archaeological site in Argentina.

1. Introduction

GPR antennae have limited directivities, with wide cones of illumination (e.g. Jiao et al., 2000; Radzevicius et al., 2003). As a consequence, an important fraction of the transmitted energy is lost outside the transmitter–reflector–receiver path, thus reducing the possibilities of detection, especially in cases with low signal to noise ratios (i.e. deep targets, high absorptions or low contrasts of dielectric permittivity). This energy loss reduces the effectiveness of the GPR methodology when using single transmitting/receiving antennae and a constant distance between them (constant offset).

The detection and interpretation of signals from buried targets can be improved by using multi-offset methodologies: CMP (common midpoint); sometimes WAR (wide-aperture reflection); AVO (amplitude variation with offset); or AVA (amplitude variation with angle) the most usual in GPR (e.g. Baker, 1998; Pipan et al., 1999; Nakashima et al., 2001; Jordan et al., 2004; Carcione et al., 2006; Berard and Maillol, 2007). An alternative way of improving the signal to noise ratio is to concentrate the available energy on the targets of interest by increasing the directivity of the transmitted fields. This increment can be obtained by using a set of closely spaced transmitting antennae, which form an array. In this case the phase, distance and amplitude relations among the antennae should be carefully selected in order to adequately narrow the transmitted fields and to direct them towards the target. Similar results can be obtained with a single transmitter, by consecutively placing it at the positions where the real array components would be, and then by superposing the fields of the individual records. In this approximation, differences between the emitting elements and coupling are overcome, while at the same time simpler acquisition and processing procedures are involved.

Synthetizing emitting fields is a well-known methodology in the seismic area (e.g. Stoffa et al., 2006, Shan and Biondi, 2008) and in the use of land, airplane and satellite radars (e.g. Thirion-Lefevre and Colin-Koeniguer, 2007; Wang, 2007).Nevertheless, few applications have been carried out with GPR (Lutz and Perroud, 2006).

In this paper the synthetic array method is evaluated as a means to improve GPR signals. The first goal of this article is to analyze how the method can work with this kind of data. To do this the fields of dipole-type array transmitters are modeled and their dependence on the most important parameters is analyzed: the number of dipoles; the distance between them; their relative phases and the distance from the center of the array to the evaluation point. Then, it is shown how to increase the directivity of the transmitted fields, so that the targets can be adequately illuminated by the wave-fronts and their signals reinforced. Next, two basic situations are examined using synthetic data: the first includes a small body and the second an extensive interface. For these cases, a methodology that simultaneously improves the signal to noise ratio and the lateral coherence of the main events is evaluated. The analysis is then extended to a situation that combines both geological models. Finally, the methodology is used to experimentally investigate a real case for which single transmitter surveying had given confusing results. This study concerns the measurement of the width and depth of mud walls at an archaeological site in Argentina.

* Corresponding author. Departamento de Física, Facultad de Ciencias Exactas y Naturales, Universidad de Buenos Aires, Ciudad Universitaria, Pabellón 1, (1428) Buenos Aires, Argentina. Tel.: +54 11 4576 3353; fax: +54 11 4576 3357.
E-mail address: bonomo@df.uba.ar (N. Bonomo).

0926-9851/$ – see front matter © 2010 Elsevier B.V. All rights reserved.
doi:10.1016/j.jappgeo.2010.01.004

2. Fields produced by synthetic dipole-type array transmitters

GPR systems often use dipole-type antennae to transmit the electromagnetic fields into the ground and to receive them. As occurs with any other kind of antennae, the transmitted fields depend on the characteristics and orientation of the emitter and the constitutive and geometrical characteristics of the air–soil interface and subsequent layers. In the case of a transmitting array, the resultant fields also depend on so-called array parameters: the relative positions of the array elements and their relative amplitudes and phases.

In this section the fields produced by synthetic dipole-type array transmitters are analyzed as functions of the array parameters that are more relevant to the effective application of the emitting-array method to GPR (next section). With respect to this, the analysis of dipole arrays located at homogeneous (infinite) spaces have shown that the spacing between the transmitters should be less than a wavelength in order to obtain a single, well defined maximum and a higher number of dipoles produce narrower beams (Lutz and Perroud, 2006). Furthermore, the phase shift between the dipoles should be selected according to the desired main-lobe direction, in order to intensify the reflected amplitudes.

When the air–soil interface is considered in the formulation, the resultant expressions for the field transmitted by a dipole cannot be solved in a closed manner (Sommerfeld, 1964). In such cases, numerical calculations are required. It should be noted that in shallow prospecting the targets often spread throughout the entire range of investigation depths, i.e. from near to far field situations, so asymptotic expressions for the responses are not applicable and the complete fields should be considered in the calculations.

The analysis begins by considering n equally spaced dipoles located at the air–soil interface as shown in Fig. 1. The dipole axes are parallel to the y-axis and perpendicular to the survey lines (along x-axis). The distance between the dipoles is denoted by d (array length $=(n-1)\,d$), and the central frequency of the emitted signal by f_c. The $z \geq 0$ medium is characterized by a relative permittivity ε_r and a conductivity σ.

Fig. 2a shows the y-component of the electric field produced by a single dipole-type source located at $x=0$, for a constant time $t=10$ ns after a pulse has been emitted. The fields are simulated by applying a 2D finite-differences code (Irving and Knight, 2006) for the TM mode. Although the radiation patterns and geometrical spreading of realistic dipole-type GPR antennae cannot be properly modeled with this 2D code (since a fully 3D approach would be necessary) we can obtain the main relevant features of the transmitted fields by applying it. In the model for Fig. 2a the soil is characterized by $\varepsilon_r=4$, $\sigma=1$ mS/m. The source wavelet is the normalized first derivative of a Blackman–Harris window function (see Irving and Knight, 2006, Fig. 2), and the source point is located at the first row of the soil portion of the grid. The central frequency of the transmitted pulse is $f_c=500$ MHz, with a bandwidth $\Delta f=1$ GHz. The dominant wavelength of the wavelet is $\lambda=0.3$ m. At an infinite uniform medium, the radiation pattern of the source is homogeneous. It can be observed in Fig. 2a that, as a consequence of the presence of the air–soil interface, the transmitted body wave presents rather constant amplitude for most of the angular range, and two weak local maxima at propagation angles of plus and minus 45° with the vertical.

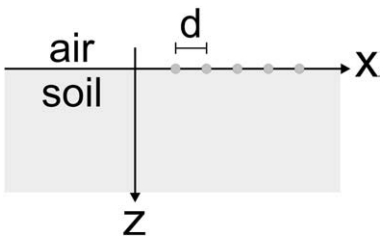

Fig. 1. Dipole geometry for a transmitting array. The distance between the dipole elements is denoted by d.

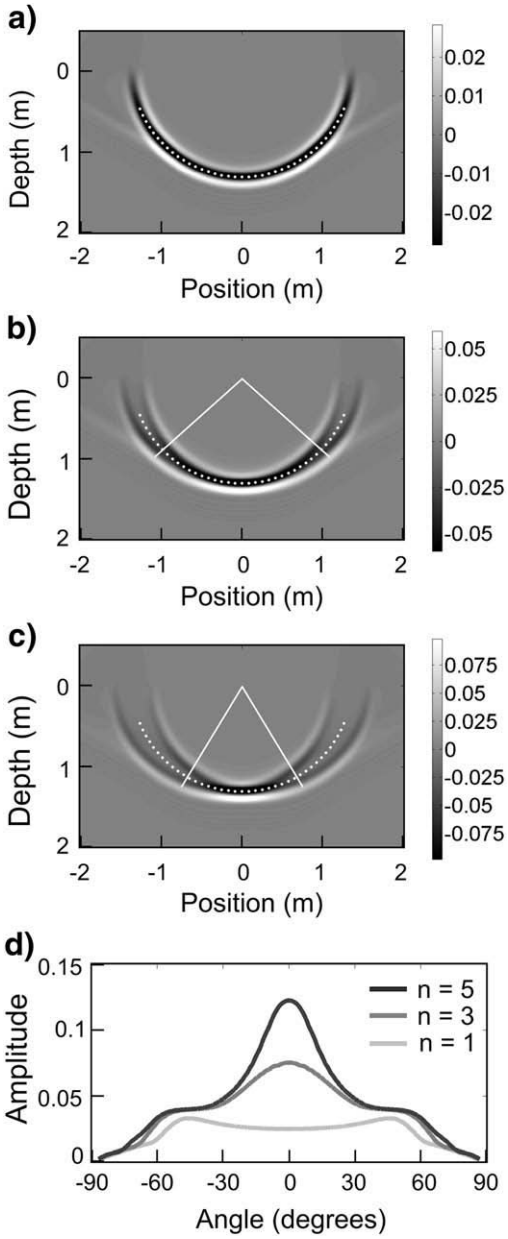

Fig. 2. Transmitted y-component of the electric field at a constant time $t=10$ ns after the emission, for different kinds of sources. a) Single dipole transmitter, b) 3-dipole array, c) 5-dipole array. In the last cases, the distance between the dipoles is $d=0.1$ m, the relative time shifts $d\tau=0$ ns, and the relative amplitudes $da=1$. The dotted line contours the wave-front of a single transmitter. The parts where the forms of the array and single transmitter wave-fronts resemble each other have been also indicated. d) Amplitudes of the wave-fronts in a to c as functions of the angle of propagation.

Fig. 2b shows the y-component of the electric field produced by the superposition of the fields produced by three dipoles. The array is centered at the origin and the distance between the dipoles is $d=0.1$ m. In this case the three dipole sources are triggered simultaneously (relative time shifts $d\tau=0$ ns), and the relative amplitudes are $da=1$ for all array elements. For an easier comparison, the dotted line in the figure contours the wave-front of a single transmitter. By comparing Fig. 2a and b it can be observed that the field of the array is more intense and concentrated around the normal direction to the interface than the field of a single transmitter. The form of the array wave-front resembles that of a single dipole within its central part, which is the most intense (between plus and minus

Please cite this article as: Cedrina, L., et al., An application of the synthetic emitter-array method to improve GPR signals, Journal of Applied Geophysics (2010), doi:10.1016/j.jappgeo.2010.01.004

48° directions approximately). For angles in the peripheral regions, both wave-forms tend to differ. Note that the concentrating effect becomes more pronounced when n is increased, as for example in Fig. 2c with $n=5$, whereas the two small local maxima in Fig. 2a ($n=1$) tend to disappear. For an easier comparison, Fig. 2d shows the amplitudes of the wave-fronts in Fig. 2a to c, as functions of the angle of propagation. In general, close to the array, the width of the central portion of the propagating array wavefield increases with n while at a few array-lengths this relation reverses, decreasing the width as n increases. The first effect is a consequence of increasing the length of the array, which naturally produces a wider field close to the emitting elements. Moreover, the resultant array wave-fronts tend to be flattened in the central part when the number of dipoles is increased. The second effect occurs because the transmitted fields present an approximate form of diverging beam, with a diminishing divergence for increasing values of n.

Deviations with respect to the single transmitter behavior also increase as z decreases, keeping constant the other parameters. An approximate explanation of this behavior is that, while reducing z, the individual wave-path lengths (from each dipole to the evaluation point) increasingly differ with respect to the wavelengths of the propagating electromagnetic field, so the individual fields interfere in more complex ways and the resultant wave-form become more complicated. This effect can clearly be observed, for example, when comparing Fig. 3a and b, which are snapshots of the transmitted fields for $t=5$ ns and $t=15$ ns. It has the same array and interface parameters as in Fig. 2c. A similar behavior can be observed when comparing Fig. 3c and d, which correspond to a distance $d=0.2$ m between the array elements (instead of $d=0.1$ m, as in the previous figures). On the other hand, when the dependence on d is analyzed (keeping constant the other parameters), it can be observed that the transmitted beam becomes less divergent for greater values of this parameter, so the resultant field narrows at evaluation surfaces far from the array. Increasing the array length also produces a wider field close to the array (as in the case of a rising n). These effects can be observed respectively when comparing Fig. 3b and d, for an evaluation surface far from the array (distance from the center of the array to the evaluation points: 2.2 m, approximately). Fig. 3a and c illustrates a situation with a surface closer to the array (approximate distance 0.7 m). From these comparisons it can also be noted that the individual fields begin to become evident in peripheral regions when d is raised because of the greater differences between the individual wave-path lengths, as previously explained, and that the central part of the array field increasingly differs with respect to the single transmitter wave-front.

Also a time shift $d\tau$ on the array has an effect on the resultant array wave-fronts. For example, in Fig. 4 the field produced by a 5-dipole array is shown, with relative time shifts $d\tau=0.1$ ns among their elements. For the mth dipole, the total time delay is given by $\tau_m=md\tau$, with $-2\le m\le 2$ and $m=0$ referring to the central dipole. The other parameters in Fig. 4 are $d=0.1$ m and $t=15$ ns. It can be observed that the most evident effect of applying the time shift is that the direction in which the transmitted beam propagates has changed. Positive $d\tau$ produces beams propagating towards the negative x-direction, whereas negative values of $d\tau$ produce beams propagating towards the positive x-direction. The angle of transmission, defined from the maxima of the field to the normal direction to the interface, in this case is $-7.4°$. It can be also noted from the figure that the transmitted wave-front approximately maintains its original form (compare Figs. 4 and 3b to check this) and that it has been laterally displaced along the single transmitter reference curve.

3. Application of the synthetic transmitting array method to GPR examples

In this section it is shown how the synthetic array method can work with GPR data and in which way their results are enhanced. The method is applied to two basic situations, one containing a small reflector and the other including an extensive surface. Subsequently, a third situation that includes a more complex geometry is analyzed.

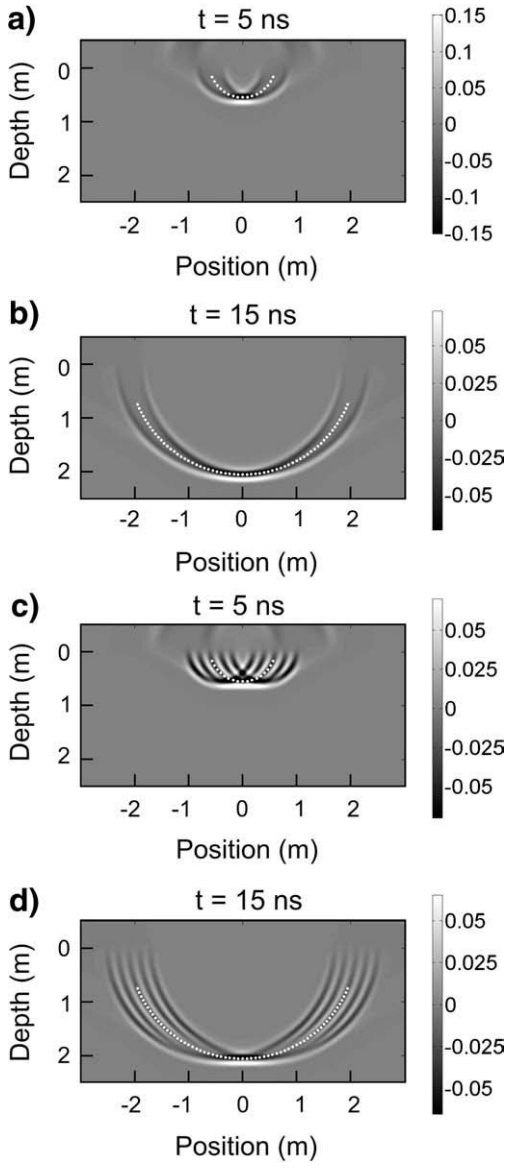

Fig. 3. Transmitted y-component of the electric field for a 5-dipole array, and for different evaluation times and distances between the dipoles. a) $d=0.1$ m, $t=5$ ns, b) $d=0.1$ m, $t=15$ ns, c) $d=0.2$ m, $t=5$ ns, d) $d=0.2$ m, $t=15$ ns.

As a general methodology to evaluate the array method, the resultant radargrams are compared with those of the single transmitter methodology. Note that both kinds of radargrams are comparable provided that the central portions of the array wave-

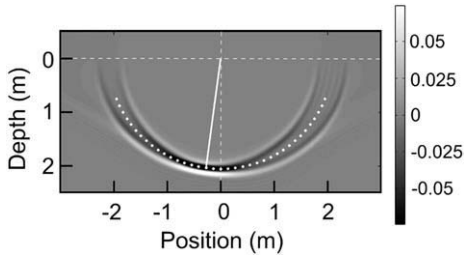

Fig. 4. Snapshot of the transmitted y-component of the electric field, for a 5-dipole array with relative time shift $d\tau=0.1$ ns between their elements. The other parameters are $d=0.1$ m and $t=15$ ns. The angle of transmission is $-7.4°$.

Please cite this article as: Cedrina, L., et al., An application of the synthetic emitter-array method to improve GPR signals, Journal of Applied Geophysics (2010), doi:10.1016/j.jappgeo.2010.01.004

fronts and the single transmitter wave-fronts have similar shapes at the target positions. As seen in the previous section, for given soil and frequency spectrum, the array wave-fronts depend on the number of constituent elements in the array, the distance between them, their relative phases and the distance from the array to the evaluation point. As a consequence, a relatively large number of parameters have to be adjusted in order that the array wave-forms resemble the single transmitter wave-forms.

Once the transmission parameters have been chosen for a particular example, constant-offset radargrams are generated for the single source and the transmitting array cases. To do this, a transmitter is located at a fixed position on the ground and the response is simulated with a finite-differences code (Irving and Knight, 2006). Traces are recorded at different points throughout the ground interface, thus obtaining a first common transmitter gather. Then, the transmitter is moved a distance d (the minimum distance between the array components) to obtain the next common transmitter gather. In this way a gather is computed for each position of the transmitter. The constant-offset GPR section is then simply obtained by extracting a trace from each gather (the trace that corresponds to the selected offset), and by presenting all the extracted traces as functions of the emitter position or, equivalently, the midpoint between the emitter and receiver positions. On the other hand, to obtain the correspondent radargram for the array, the common emitter traces are rearranged in common receiver gathers. For each receiver gather, n traces that correspond to the n components of the array (the "offset" is defined with respect to the central element of the array) are extracted. Then time delays t_m are applied to the n traces in each set and a summation is performed. Finally, the synthesized traces are sorted and presented together, as functions of the receiver or midpoint positions.

As mentioned above, the first basic example concerns the reflection at a small object. The input model is shown in Fig. 5a. The diameter of the object is 0.1 m, and the depth from the surface to the top of the target 0.75 m. The permittivity and resistivity of the soil are $\varepsilon_r = 4$ and $\sigma = 1$ mS/m, respectively, whereas for the body $\varepsilon_r = 5$ and $\sigma = 2$ mS/m. Random noise 10% is applied to the constitutive parameters of both media throughout the grid (grid increment 1 cm). The emitted fields have central frequency 500 MHz ($\lambda \approx 0.3$ m), with an approximate bandwidth 1 GHz.

Fig. 5b shows the single transmitter radargram for the model in Fig. 5a, when a constant offset 0.5 m is considered. In this case, the transmitter is disposed to the right of the receiver (RE configuration). The x coordinate in the graph refers to the midpoint between the emitter and receiver positions. A typical inverted U-shape signal can be observed in the figure (a "diffraction" signal), which corresponds to the reflection at the buried object. Likewise, Fig. 5c shows the radargram that results for a 5-source array, with $d = 0.1$ m, $d\tau = -0.2$ ns. It has the same offset as that in Fig. 5b. The non-zero time shift makes the transmitted beam propagate along a direction $\theta = 17.2°$ with respect to the normal direction to the air–soil interface. As in the case of the single transmitter, the array components are disposed to the right of the receiver, whereas the x coordinate refers to the midpoint between the central source and the receiver positions. By comparing Fig. 5b and c it can be observed that, in the case of the array, the reflection signal has been intensified in the x-interval (−0.8 −0.2) m, approximately, and attenuated outside it. This simply occurs because the transmitted beam centrally illuminates the body within this interval, and marginally illuminates the target outside it. The signal to noise ratio increases up to 193% (143% on average) inside the interval as a consequence of diminishing the intensity of noise arriving from peripheral portions of soil since they are faintly illuminated. This result also occurs due to the averaging of traces, which tend to cancel random and high spatial-frequency noise and reinforce primary reflections originated in the centrally illuminated fringe. Considering these dependences, increments in directionality and number of elements in the array would be convenient to improve the signal to noise ratio. Nevertheless, note that n and d should be low enough to assure adequate down-going wave-fronts, as explained in the previous section.

In Fig. 5d to f the values of $d\tau$ are varied, keeping constant the other array parameters. This is equivalent to changing the transmission angle. The used $d\tau$ values are 0 ns, 0.2 ns and 0.4 ns, respectively. It can be verified how consecutive portions of the diffraction signal are highlighted by changing $d\tau$. As mentioned above, a portion of the signal is highlighted when the transmitted beam is directly orientated towards the target, thus centrally illuminating it. Similarly, different portions of the signals that correspond to the fluctuations in the geological model are intensified when $d\tau$ varies. For a given $d\tau$, the intensified portions have similar slopes. As a consequence, parallel fringes could result in the constant $d\tau$ radargrams in sectors in which the approximately-aligned highlighted portions appear. A number of constant slope fringes can clearly be observed throughout Fig. 5c to f.

The previous examples have shown that the synthetic array method is useful for improving different parts of the primary signal from the small reflector, when the angle of transmission is varied. Nevertheless, when considering real radargrams, in which many different signals closely coexist, it is necessary to highlight the complete signal from the diffractor so that it can be adequately detected and interpreted. This is equivalent to improving the lateral coherence of the highlighted signal. The examples above give an idea of how to do this. A tentative procedure could be the following: 1) generate a set of radargrams, for different values of $d\tau$, 2) in each of them determine a segment in which the signal is clearly improved, and the respective x-interval, 3) cut out the portion of radargram that corresponds to the interval, 4) if necessary, crop bordering traces so that non overlapping intervals result, 5) sort the resultant pieces of radargram and present them together.

The radargram that results from applying the described procedure to the model in Fig. 5a is shown in Fig. 5g. The complete diffraction signal has been improved and the global signal to noise ratio has increased (154% on average). It can also be noted that the consecutive appended sections perfectly match. This occurs because an adequate set of transmission parameters (n, d) has been selected, i.e. the transmitted wave-fronts have similar forms to single-source wave-fronts at the target position. Moreover, small enough increments in $d\tau$ and proper imaging segments of radargrams have been selected.

The second basic example is the case where the reflection is generated at an extensive subsurface interface. Fig. 6a shows the input model set up. The upper layer is characterized by $\varepsilon_r = 4$ and $\sigma = 1$ mS/m, and the deeper medium by $\varepsilon_r = 5$ and $\sigma = 2$ mS/m. The reflector is located at an average depth of 0.9 m. Fig. 6b depicts the single transmitter radargram, for an offset of 0.5 m and the receiver to the left of the emitter (RE configuration). The dominant frequency of the source is 500 MHz, whereas 10% random noise has been applied to the grid distributions of constitutive parameters.

Fig. 6c shows the 5-element array radargram for the model in Fig. 5a, when $d = 0.1$ m and $d\tau = 0$ ns. Due to this value, the transmitted central beam propagates along the vertical direction. By comparing Fig. 6b and c, it can be observed that the left and central parts of the signal, which are respectively related to the left dipping and central horizontal segments of the interface, have their amplitudes augmented. For these portions, the signal to noise ratio increases 172% and 143%, respectively. On the other hand, it can be observed that the response from the right dipping segment becomes blurred. The method has efficiently intensified the left part of the signal since the transmitted beam reflects at the corresponding plane directly towards the receptor, or very close to it, so that maximum amplitudes are obtained. The part of the signal related to the horizontal central plane has lower intensity, due to an increasing distance between the maximum of the reflected beam and the receiver. Finally, the method is not effective for the dipping right segment, since in this case only a peripheral part of the reflected beam reaches the receptor.

Please cite this article as: Cedrina, L., et al., An application of the synthetic emitter-array method to improve GPR signals, Journal of Applied Geophysics (2010), doi:10.1016/j.jappgeo.2010.01.004

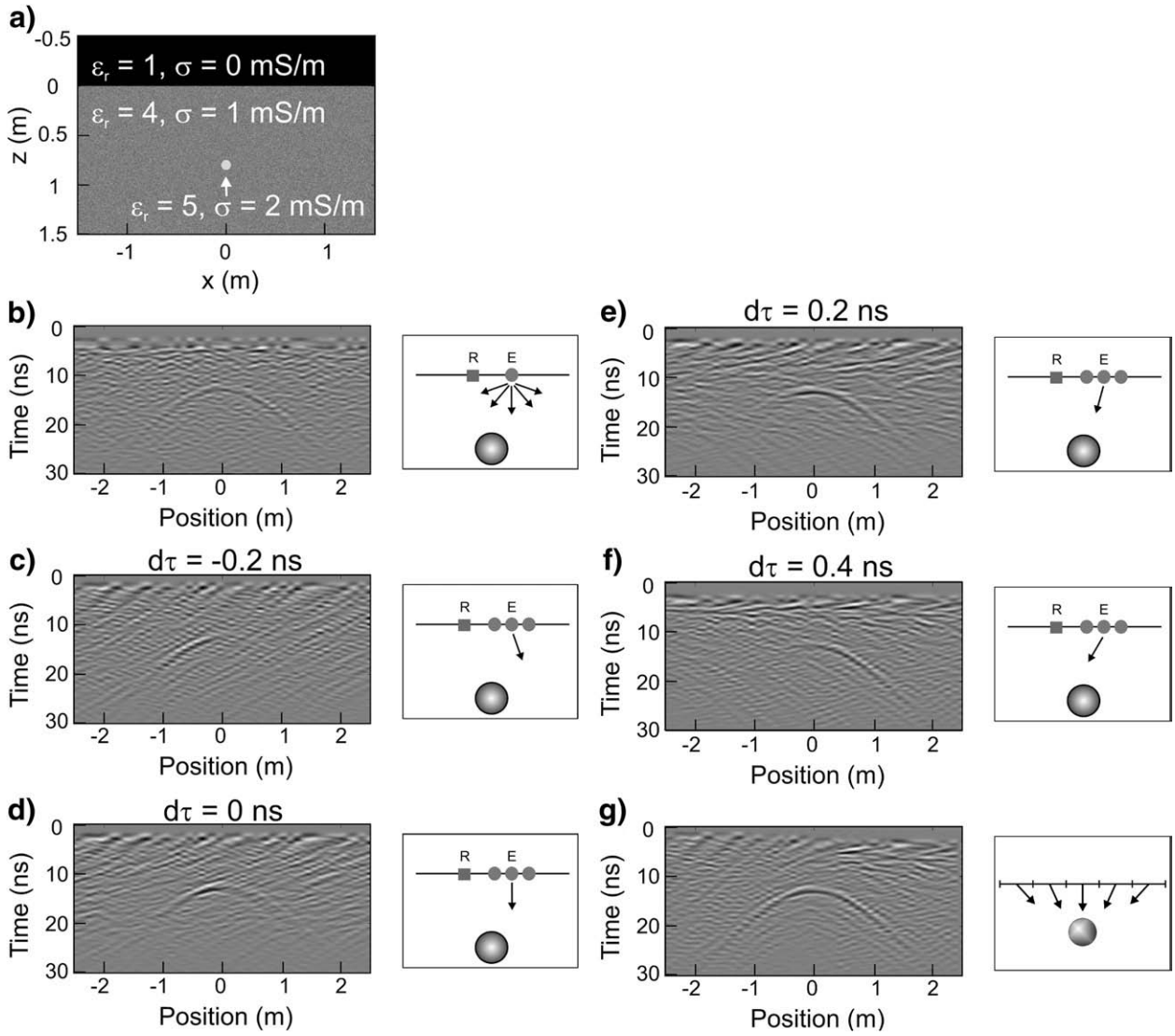

Fig. 5. a) Reflector 0.1 m in diameter, located at a depth 0.8. The surrounding media is characterized by $\varepsilon_r = 4$ and $\sigma = 1$ mS/m, whereas the object by $\varepsilon_r = 5$ and $\sigma = 2$ mS/m. b) Single source radargram (y-component of the electric field) for a constant offset 0.5 m (RE configuration). The x-axis refers to the midpoint positions, as in the next figures. c) Synthethic 5-source radargram, for an array with $d = 0.1$ m and $d\tau = -0.2$ ns, d) $d\tau = 0.0$ ns, e) $d\tau = 0.2$ ns, f) $d\tau = 0.4$ ns. g) Radargram obtained by appending portions of the previous radargrams. 5 approximately equal intervals have been used in this process.

As in the case of the small diffractor, other portions of the reflection signal can be highlighted by varying the time shift $d\tau$. For example, $d\tau = 0.15$ ns is used in Fig. 6d, and $d\tau = 0.3$ ns in Fig. 6e. It can be verified how the central and right parts of the signal are respectively highlighted in these figures. Next, the procedure is applied to evaluate whether the entire signal from the extensive reflector can also be improved. Fig. 6f shows the results of this procedure. It can be observed that the reflected signal presents a similar aspect to the original (Fig. 6b), thus maintaining the level of coherence, but with a higher signal to noise ratio (210% on average). This result illustrates the efficiency of the methodology also in the modeled case of an extensive reflector.

Taking into account the results obtained for the small diffractor and the extensive reflector cases, the following procedure to improve a signal is proposed:

1) Select a target response from a single transmitter radargram (a diffraction signal or a reflection),
2) Divide the object generated signal into approximate segments, to which the array method will be applied. In the horizontal plane portions of the signal, the segments can be chosen as large as these portions; in curved or dipping parts, the segments should be smaller so that an improved lateral continuity is obtained through the method,
3) Obtain a series of array radargrams by varying the time shift $d\tau$ between the elements in the array,
4) In each segment, determine for which $d\tau$ the signal is best improved,
5) Subdivide segments if necessary,
6) Cut out the portions of radargrams that correspond to the resulting improved segments and put them together to obtain the final radargram.

In experimental situations it is usual that parts of the original signal cannot be clearly defined due to the low signal to noise ratio. In these cases, tentative segments should be considered in step 2. Although a single segment could be sufficient to link two separate parts of a signal, in many cases it is necessary to use larger numbers of them; the amount depends on the reflector complexity. A complex situation occurs when it is unclear how a signal continues at the other side of a confusing area, i.e. with which signal it has to be linked (for example, when various thin strata coexist). In these cases, too small sweep ranges or large increments for the time shift could skip relevant

Please cite this article as: Cedrina, L., et al., An application of the synthetic emitter-array method to improve GPR signals, Journal of Applied Geophysics (2010), doi:10.1016/j.jappgeo.2010.01.004

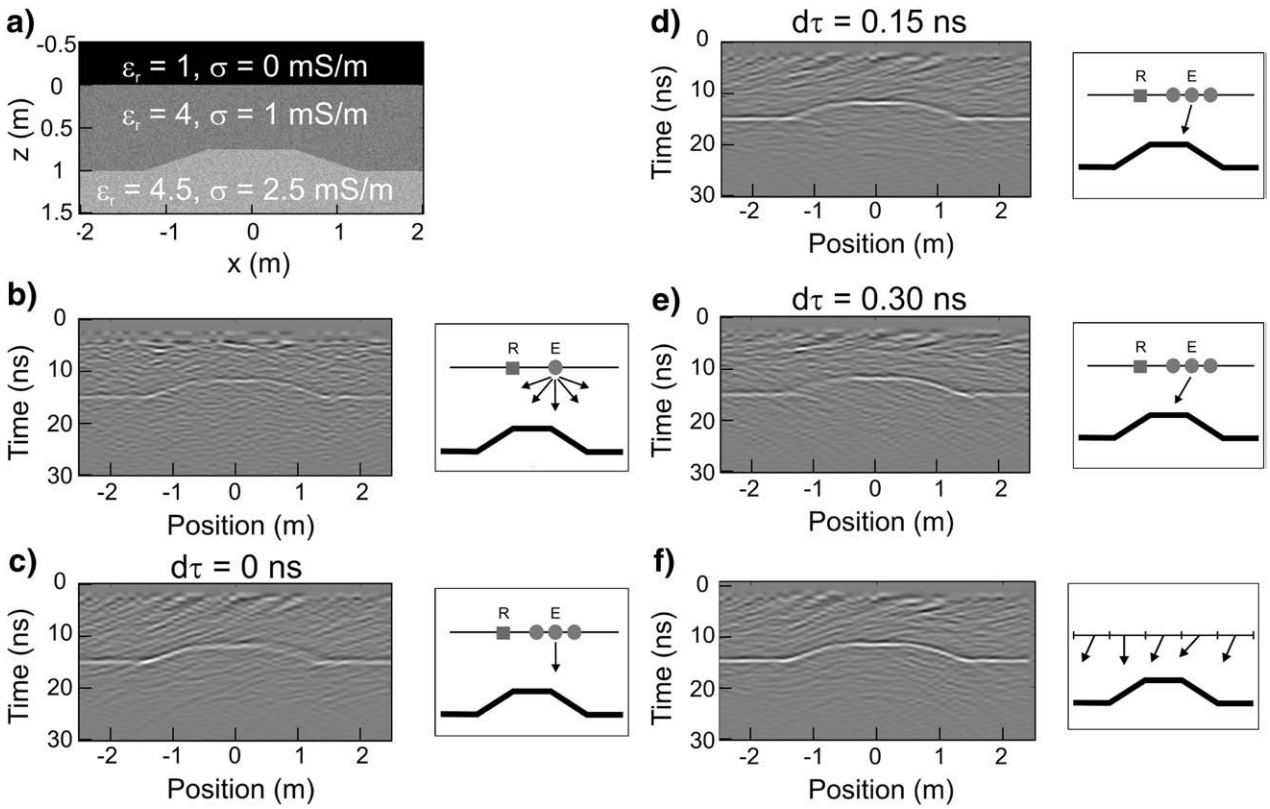

Fig. 6. a) Model with an extensive reflector ($\varepsilon_r = 4$ and $\sigma = 1$ mS/m for the shallower layer; $\varepsilon_r = 5$ and $\sigma = 2$ mS/m for the deeper layer), b) single transmitter radargram (y-component of the electric field, offset 0.5 m, RE configuration), c) 5-element array radargram for $d\tau = 0$ ns and $d = 0.1$ m, d) the same as in c, but with $d\tau = 0.15$, e) $d\tau = 0.30$, f) radargram obtained by appending portions of radargrams with different $d\tau$.

portions of the signal to be improved, so that the methodology could fail or give rise to incorrect conclusions. Then, in step 3, it is convenient to select a wide range for $d\tau$ and an increment as small as the sampling period or even below it. In this case the traces will require interpolation. Other complex situations are those in which two or more signals superimpose inside an interval. In these cases only one branch at a time can be improved using this methodology.

Before considering an experimental case, a final numerical example is examined. Fig. 7a shows the model, which includes two small diffractors and an extensive reflector, located at depths 0.5 m and 1.0 m, respectively. Both diffractors are characterized by a diameter 0.1 m, $\varepsilon_r = 5$ and $\sigma = 1.5$ mS/m. The shallower stratum is characterized by $\varepsilon_r = 4$ and $\sigma = 1$ mS/m, and the deeper stratum by $\varepsilon_r = 4.2$ and $\sigma = 2.5$ mS/m. The dominant frequency of the source is 500 MHz, and a 10% random noise is applied to the permittivity and resistivity matrixes. Fig. 7b shows the radargram for a single transmitting element, with offset 0.5 m and RE configuration. Although the signals from the diffractors can be seen clearly, the reflection at the buried interface is fairly weak. In such cases the array methodology can be applied in order to improve visibility. To do this, a 5-element array is used with $d = 0.1$ m, the other parameters being the same as in the previous figure. A set of temporal shifts between 0.00 ns and 0.15 ns, with increment 0.05 ns has been utilized in this case. The resulting radargram in Fig. 7c confirms that the quality of the signal of interest has been successfully improved. Note that the signals from the small reflectors have been highlighted only in small portions, but that they are more blurred as a whole. In this sense, it is clear that diffraction signals tend to be filtered out by the method when it is applied to enhance the signal from an extensive reflector. Alternatively, the signal from one of the small targets can be improved. For example, Fig. 7d highlights the signal from the right diffractor. Note that in this case the signal from the deeper layer almost disappeared. This is because the beams are disposed of in order to reflect the energy in the small targets directly towards the receiver, whereas the energy reflected in the layer is mainly directed outside it. As a final example in Fig. 7e both diffractors are highlighted. To do this, a technique that consists of dividing the x-range into halves is used; in each half the array methodology is applied to the respective diffraction signal, with subsequent visualization of both results at the same time.

4. Field example

According to the results in the preceding section, the synthetic array method is a useful tool to investigate the behavior of reflectors that present faint or doubtful GPR signals. Similar to other methods comprising variable offset data, the array methodology requires a considerable time for acquisition, so it is important to carefully select the portions of soil to be investigated. A previous constant-offset prospecting survey is very useful in evaluating the quality of the reflection signals and restricting the volumes of soil to be considered, thus minimizing the study efforts.

The benefits of the array methodology are demonstrated in this section by applying it to determine the width and depth of mud walls at the archaeological site of Palo Blanco, Catamarca province, Argentina. This site is related to one of the first agricultural/pastoral communities of the region, which mainly developed during the Formative Period, approximately 1500–1700 years ago. Knowing the values of these parameters (width and depth of the walls) is very important to the archaeologists since they perform comparative studies, statistical analysis, etc. Furthermore, the depth values are relevant to calculate the amount of soil to be removed when planning an excavation.

In 2007 an extensive geophysical prospecting at Palo Blanco site was performed by using a fast constant-offset GPR acquisition methodology. The analysis of the data provided a detailed map of the archaeological buried structures, particularly, a number of mud

Please cite this article as: Cedrina, L., et al., An application of the synthetic emitter-array method to improve GPR signals, Journal of Applied Geophysics (2010), doi:10.1016/j.jappgeo.2010.01.004

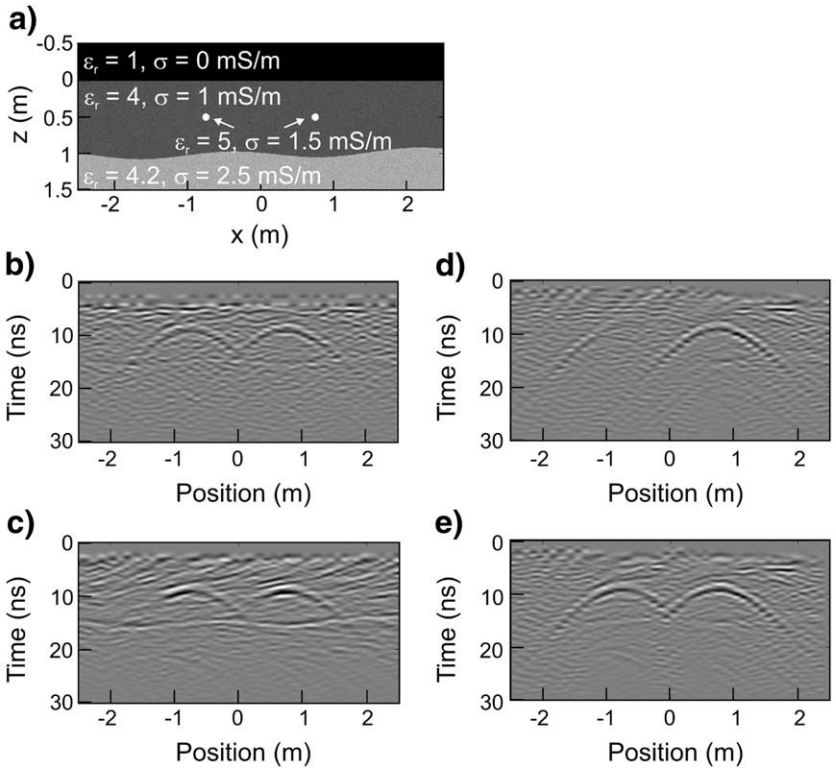

Fig. 7. a) Model. The diffractors have diameters 0.1 m, $\varepsilon_r = 5$ and $\sigma = 1.5$ mS/m. The shallower stratum is characterized by $\varepsilon_r = 4$ and $\sigma = 1$ mS/m; the deeper stratum by $\varepsilon_r = 4.2$ and $\sigma = 2.5$ mS/m. 10% random fluctuations are applied to these parameters. b) Single transmitter radargram (*y*-component of the electric field) for a central frequency 500 MHz. c) 5-element array radargram obtained by appending portions of radargrams with different dτ, so that the horizontal interface is improved. d) Composed 5-element radargram in which the signal from the right diffractor is highlighted. e) The *x*-axis is divided into halves, and the methodology is applied to improve the respective diffraction signal.

walls that defined a complex layout of rooms and possible courtyards (Martino et al., 2005). Although the lateral position of the walls was precisely established through the initially applied GPR methodology, only imprecise values for the wall widths were obtained with rather doubtful measures for their depths at a few short sections of the walls. These uncertainties are in the first place consequences of the moderate to low permittivity contrasts occurring at the target interface. This is mainly because the original inhabitants constructed the walls with the same surrounding materials. Secondly, the bottoms of the walls normally present smooth transitions in the permittivity due to the compressing and natural drying processes during their building.

Fig. 8a shows a single transmitter radargram, for a survey line performed across one of the walls detected at Palo Blanco. In this example, the offset is 0.5 m, and the configuration has been set to RE. It can be checked that neither the lateral limits nor the bottom of the wall can be precisely established from this radargram. Only a signal at approximately 17 ns seems to indicate the bottom of the wall, although it is too weak and incomplete to ascertain this. The array methodology is first applied to improve the reflection from the bottom and then to better define the diffraction signals at the edges of the walls. This result enables indirectly measuring the wall widths. A 5-element array is deployed with spacing $d = 0.1$ m between them. The offset value is 0.5 m and the configuration RE, as in previous figures. Following the explained methodology, the transmitted illumination beam is directed towards the bottom of the wall and the time shift is varied (from −0.30 ns to 0.30 ns, with increment 0.05 ns), so that all the relevant parts in the signal are improved. After selecting the most adequate time shifts for each segment of signal, the superposition is performed. The resultant radargram is shown in Fig. 8b. It can be observed that the applied procedure has effectively highlighted the event around 17 ns, completing the signal across the wall. In this manner, the bottom of the wall has been properly delimited.

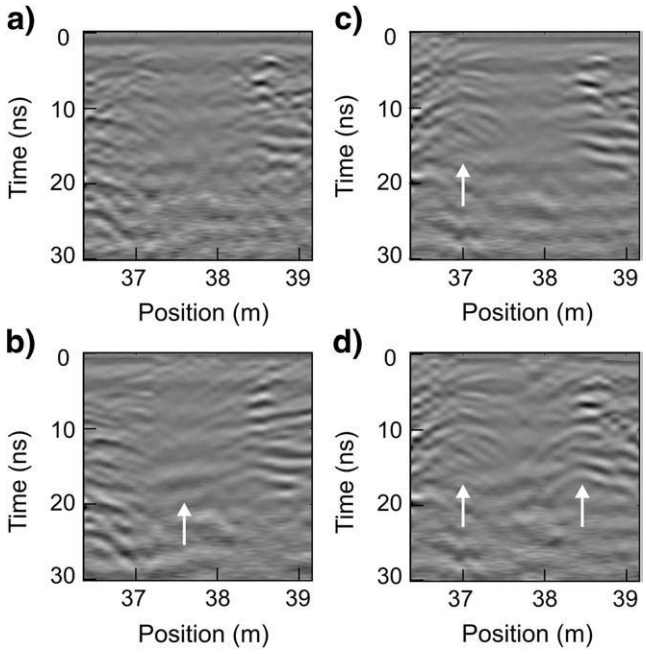

Fig. 8. a) Single transmitter radargram for a survey line performed across one of the walls detected at Palo Blanco. The offset is 0.5 m, the configuration is RE, and the central frequency is 500 MHz. b) Composed 5-element array radargrams ($d = 0.1$ m; offset = 0.5 m), for a set of time shifts between −0.30 ns and 0.30 ns, with increment 0.05 ns. c) Composed 5-element radargram that highlights the diffraction signal with vertex at $(x, t) = (37$ m, 8 ns). d) The *x*-axis is divided into halves, and the methodology is applied to the diffraction signals with vertices at $(x, t) = (37$ m, 8 ns) and $(x, t) = (38.5$ m, 10 ns).

Please cite this article as: Cedrina, L., et al., An application of the synthetic emitter-array method to improve GPR signals, Journal of Applied Geophysics (2010), doi:10.1016/j.jappgeo.2010.01.004

Fig. 8c is an example of how a diffraction signal from one of the edges of the wall can be improved. The highlighted signal can be identified easily in the figure; the position of its vertex is approximately $(x,\ t) = (37\ \text{m},\ 8\ \text{ns})$. It can also be noted that other surrounding diffraction signals have been improved, since the transmitted field has a finite width. Finally, in Fig. 8d an example is given in which opposite diffractors have been highlighted by dividing the x-axis into halves and by applying the array methodology to each of them, as explained in the previous section. The left highlighted signal is the same as that in Fig. 8c whereas the right signal has its vertex at $(x, t) = (38.5\ \text{m}, 10\ \text{ns})$. It can also be observed in the figure that a number of diffraction signals, whose vertices are located along a vertical fringe around $x = 38.5$ m, have been improved by the method, thus contributing to delimiting the right border of the wall.

5. Conclusions

The synthetic emitting-array method has been examined as a way to improve GPR signals. The synthetic array fields have been built by superposing the fields of a single source that is consecutively placed at the positions where the real array elements would be.

The fields of dipole-type emitting-arrays have been simulated and analyzed in order to effectively apply the methodology to different kinds of GPR targets. The effects of the main parameters of the array and the distance from the array to the target on the wave-fronts were considered. It has been illustrated how the array wave-fronts become increasingly different with respect to the single transmitter case for a larger number of emitters, n, which results in very complex or incomprehensible radargrams, so that the maximum value for n is in fact constrained. In real experimental cases n is also restricted by the time required for acquisition or by the number of available sources when simultaneous emission is used. Moreover, the analysis showed that the complexity of the wave-fronts increases for larger distances, d, between the dipoles and for smaller distances from the array to the evaluation points (the position of the target). Although smaller d can produce more adequate wave-fronts, this parameter is limited in experiments by the precision of the measured positions, or, alternatively, the sizes of the transmitting devices and the coupling between the antennas. Finally, the way a time shift $d\tau$ between the array elements controls the dominant direction in which the transmitted beam propagates has been shown.

It has also been explained how the synthetic array method works with different kinds of GPR targets and in which manner their results can be enhanced. Two fundamental situations have been considered, one containing a small reflector and the other including an extensive interface. Different parts of the reflected signals were highlighted by varying the angle of transmission, whereas the other parts of the target signals attenuated. The intensified parts correspond to those portions of buried interface that directly reflect the energy towards the receiver; the other parts correspond to segments that are faintly illuminated or that reflect the beam outside the receiver position. The signal to noise ratio was effectively increased for the highlighted parts of the signal. The improvement is a consequence of reducing the amount of noise received from regions of soil that are slightly illuminated, and of averaging the events from the illuminated fringe. The latter process tends to cancel random and high spatial-frequency noise and thus to reinforce the primary reflections.

When applied in a simple manner, the array method proved efficacious for selectively improving portions of the target GPR signal but, unfortunately, it did not enhance the entire event. To overcome this deficiency, an alternative methodology that simultaneously boosts the signal to noise ratio and the lateral coherence of the target signal has been considered. The suggested workflow consists of selecting a set of time shifts (or equivalently, emission angles) for which all the relevant portions of the signal are improved. Then, the improved portions are cut out and put together in a final radargram. This methodology has been applied to a model that includes two small reflectors and a smooth interface. The example demonstrated the ability of the method to selectively improve the GPR signals of each object and to filter out the other signals. Finally, a variation of this technique to simultaneously highlight both diffractors on the resulting radargram has been applied.

The capabilities of the array method to investigate reflectors that generate only faint or doubtful signals have been demonstrated by applying it in a real case study. This test case concerns the measurement of the width and depth of mud walls at the archaeological Palo Blanco site, for which previous single transmitter GPR surveys had given negative results. The array method proved to be efficient for improving the responses and coherence of the GPR signals from the bottom of the walls and the diffractions from their lateral edges. In this manner, these archaeological features were resolved.

Acknowledgements

This work was partially supported by grants from CONICET (Consejo Nacional de Investigaciones Científicas y Técnicas) and ANPCyT (Agencia Nacional de Promoción Científica y Tecnológica).

References

Baker, G.S., 1998. Applying AVO analysis to GPR data. Geophysical Research Letters 25, 397–400.
Berard, B., Maillol, J., 2007. Multi-offset ground penetrating radar data for improved imaging in areas of lateral complexity — application at a native American site. Journal of Applied Geophysics 62, 167–177.
Carcione, J., Gei, D., Botelho, M., Osella, A., de la Vega, M., 2006. Fresnel reflection coefficients for GPR-AVA analysis and detection of seawater and NAPL contaminants. Near Surface Geophysics 4, 253–264.
Irving, J., Knight, R., 2006. Numerical modeling of ground-penetrating radar in 2-D using MATLAB. Computers & Geosciences 32, 1247–1258.
Jiao, Y., McMechan, G., Pettinelli, E., 2000. In situ 2-D and 3-D measurements of radiation patterns of half-wave dipole GPR antennas. Journal of Applied Geophysics 43, 69–89.
Jordan, T., Baker, G., Henn, K., Messier, J., 2004. Using amplitude variation with offset and normalized residual polarization analysis of ground penetrating radar data to differentiate an NAPL release from stratigraphic changes. Journal of Applied Geophysics 56, 41–58.
Lutz, P., Perroud, H., 2006. Phased-array transmitters for GPR surveys. Journal of Geophysics and Engineering 3, 35–42.
Martino, L., Bonomo, N., Lascano, E., Osella, A., Ratto, N., 2005. Electrical and GPR joint prospecting at the Palo Blanco archaelogical site, NW Argentina. A case history. Geophysics 71 (6), 193–199.
Nakashima, Y., Zhou, H., Sato, M., 2001. Estimation of groundwater level by GPR in an area with multiple ambiguous reflections. Journal of Applied Geophysics 47, 241–249.
Pipan, M., Baradello, L., Forte, E., Prizzon, A., Finetti, I., 1999. 2-D and 3-D processing and interpretation of multi-fold ground penetrating radar data: a case history from an archaeological site. Journal of Applied Geophysics 41, 271–292.
Radzevicius, S., Chen, C., Peters Jr., L., Danielsc, J., 2003. Near-field dipole radiation dynamics through FDTD modeling. Journal of Applied Geophysics 52, 75–91.
Shan, G., Biondi, B., 2008. Plane-wave migration in tilted coordinates. Geophysics 73, S185–S194.
Sommerfeld, A., 1964. Partial Differential Equations in Physics. Academic Press, New York.
Stoffa, P., Sen, M., Seifoullaev, R., Pestana, R., Fokkema, J., 2006. Plane-wave depth migration. Geophysics 71, S261–S272.
Thirion-Lefevre, L., Colin-Koeniguer, E., 2007. Investigating attenuation, scattering phase center and total height using simulated interferometric SAR images of forested areas. IEEE Transactions on Geosciences and Remote Sensing 45, 3172–3179.
Wang, W., 2007. Approach of adaptive synchronization for bistatic SAR real-time imaging. IEEE Transactions on Geosciences and Remote Sensing 45, 2695–2700.

Please cite this article as: Cedrina, L., et al., An application of the synthetic emitter-array method to improve GPR signals, Journal of Applied Geophysics (2010), doi:10.1016/j.jappgeo.2010.01.004